Numerical Simulations of Imaging Extrasolar Planets using Circular and Square Apodize Apertures

*Ali T. Mohammed** *Uday E. Jallod**

Received 24, April, 2012
Accepted 14, October, 2012

Abstract:

Numerical simulations are carried out to assess the quality of the circular and square apodize apertures in observing extrasolar planets. The logarithmic scale of the normalized point spread function of these apertures showed sharp decline in the radial frequency components reaching to 10^{-36} and 10^{-34} respectively and demonstrating promising results. This decline is associated with an increase in the full width of the point spread function. A trade off must be done between this full width and the radial frequency components to overcome the problem of imaging extrasolar planets.

Key words: Coronography, Fourier Optics, Imaging System.

Introduction:

The field of high contrast imaging has expanded in the last few years, in order to enable scientists to make direct detection and characterization of extrsolar planets. Ground - based optical imaging requires perfect correlation between coronography and adaptive optics (AO) [1]. The concept of coronography is based on observing solar corona during total solar eclipses. Lyot invented the solar coronograph (1930, 1931, and 1939). This instrument was a solar telescope equipped with a mask, it's size was exactly that of the sun. Therefore, the light coming from the sun disk was blocked. Astronomers have tried to apply this method to observe stellar structures [2, 3].

Stellar coronography is a powerful technique for the detection of a faint object around a bright source [4]. Coronography can reduce the diffracted light coming from extremely bright object to a certain level to allow search for extrasolar planets [5, 6]. A large number of coronographic concepts have been demonstrated in the last few years. They can be organized as pupil apodization, either using shaped amplitude or phase apodization [7]. Ground-based coronographs have to deal with geometrically obscured pupil function. Therefore, astronomers studied some theoretical aspects on how a coronograph can work under such constraints [8, 9, and 10].

It is planned to install stellar coronograph for the space infrared telescope for cosmology and astrophysics (SPICA) in 2018. The SPICA is an astronomical mission optimized with pupil diameter of 3.2 m. The SPICA has been designed for a concentrated study of extrasolar planets. The SPICA mission will provide us with optimum opportunity to make high dynamic range observation because of its aperture, high stability, and the capability for making infrared observations from deep space [11]. SPICA coronograph has several features. First, it targets mid – infrared region. This region has a great advantage in direct observation,

*Department of Astronomy, College of Science, University of Baghdad, Baghdad-Iraq

because the contrast between the star and planet is around 10^{-6} at mid infrared and near 10^{-10} at visible [12, 13].

The work of this paper is concentrated on numerical simulations of direct imaging of extrasolar planets using low contrast ratio. This also involves the quantitative assessment of such imaging.

Theoretical Modeling:

The general complex pupil function could be written as [14]:

$$P(\zeta,\gamma) = a(\zeta,\gamma)e^{i\emptyset(\zeta,\gamma)} \quad \dots (1)$$

where $a(\zeta,\gamma)$, $\emptyset(\zeta,\gamma)$ are the amplitude and the phase aberration of an optical system. ζ,γ are coordinates in the pupil function.

The function $e^{i\emptyset(\zeta,\gamma)}$ can be expanded using a Taylor series:

$$e^{i\emptyset(\zeta,\gamma)} = 1 + i\emptyset - \emptyset^2/2 + \dots\dots (2)$$

The medium is assumed to be a perfectly homogeneous (aberration free system), therefore equation (1) becomes:

$$P(\zeta,\gamma) = a(\zeta,\gamma) \dots (3)$$

The point spread function (psf) of any optical imaging system is the image of a point source. The electric field, $E(x,y)$, in the image plane is the Fourier transform of the pupil function, where x and y are coordinates in the image plane [15].

$$psf(x,y) = |E(x,y)|^2 \quad \dots (4)$$

the above equation could also be written as:

$$psf(x,y) = |FT(P(\zeta,\gamma))|^2 \dots (5)$$

where FT denotes Fourier transform operator. Equation (3) takes several shapes such as (circle, square, rectangular,…., ect.). The circular shape of the pupil function is given by [16]:

$$Pc(\zeta,\gamma) = \begin{cases} 1 & \text{if } \rho \le R \\ 0 & \text{otherwise} \end{cases} \dots (6)$$

where R is the radius of the optical telescope and ρ is given by:

$$\rho = ((\zeta - \zeta_c)^2 + (\gamma - \gamma_c)^2)^{1/2} \dots (7)$$

(ζ_c, γ_c) is the center of a 2-dimensional array, as shown in figure (1).

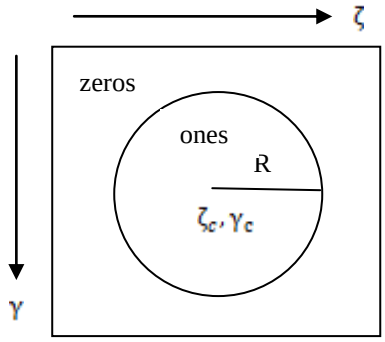

Fig. 1: The principle of implementing equations (6) & (7).

The square aperture takes the form [17]:

$$Ps(\zeta,\gamma) = \begin{cases} 1 & \text{for } |x| \le L \ |y| \le L \\ 0 & \text{otherwise} \end{cases} \dots (8)$$

Another type of aperture that presented in literature is a functional shape aperture named as apodize square aperture (ASA) [18]. This kind of aperture was suggested to reduce the diffraction limited psf to a certain value to allow an excess to detect extrasolar planet that lies beneath these diffraction frequencies.

$$ASA(\zeta,\gamma) = \begin{cases} (1-x^2)^{\upsilon-1}\,(1-y^2)^{\upsilon-1} & \text{if } -1 \le x \le 1,\ -1 \le y \le 1 \quad \text{inside } P_c \ \& \ P_s \\ 0 & \text{otherwise} \end{cases} \dots (9)$$

where υ is a small integer value.

Computer Simulations:

The pupil function P(ζ, γ) is taken to be a circular and a square function of diameter, D = 2R, and of length L respectively. The values inside these two apertures are ones according to equations (6 & 8). The size of each array is taken to be 256 by 256 pixels. This size is chosen in order to keep the diffraction limited cut off frequency to be vanish inside this array. It should be pointed out here that the diameter of the circular function is taken to be 120 pixels and the length of the square is taken to be 106 pixels. These two values produce nearly the same area for both functions (same unit area). The psf's of the above apertures are computed following equation (5) and the results are then normalized to one at their maximum values. The apertures and the corresponding psfs are demonstrated in figure (2 & 3).

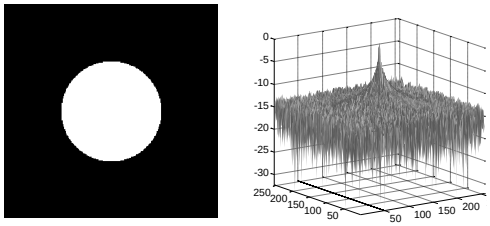

(a) (b)

Fig. 2: (a) Circular aperture (D = 120 pixels) and (b) Logarithmic scale of a normalized psf.

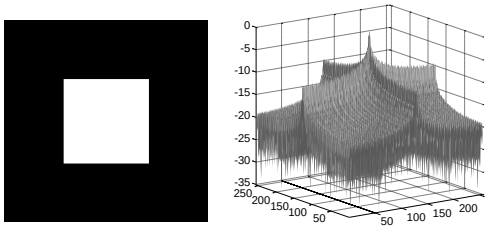

(a) (b)

Fig. 3: (a) Square aperture (L = 106 pixels) and (b) Logarithmic scale of a normalized psf.

The result of implementing equation (9) and the corresponding psf using different values of υ are shown in figures (4 to 9).

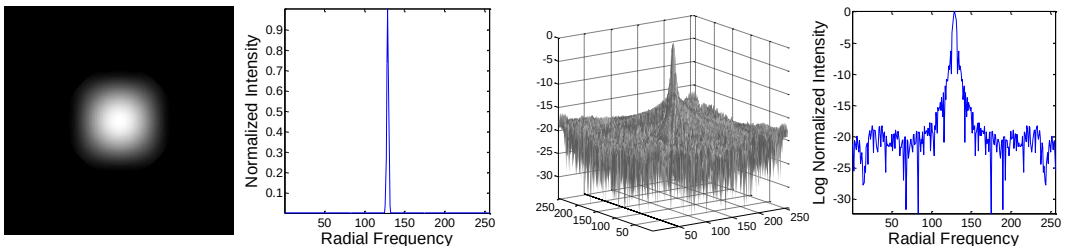

(a) (b) (c) (b)

Fig. 4: (a) Circular apodize aperture at υ =2, (b) Central line through a normalized psf, (c) Logarithmic scale of a normalized psf, and (d) Central line through (c).

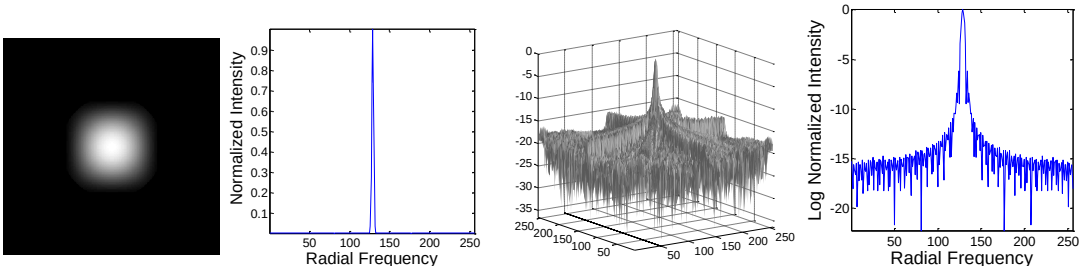

(a) (b) (c) (d)

Fig. 5:(a) Square apodize aperture at υ =2, (b) Central line through a normalized psf (c) Logarithmic scale of a normalized psf, and (d) Central line through (c).

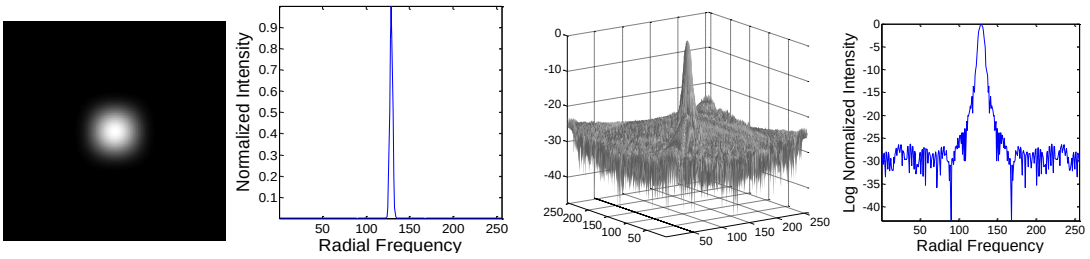

(a) (b) (c) (d)

Fig. 6: (a) Circular apodize aperture at υ =5, (b) Central line through a normalized psf, (c) Logarithmic scale of a normalized psf, and (d) Central line through (c).

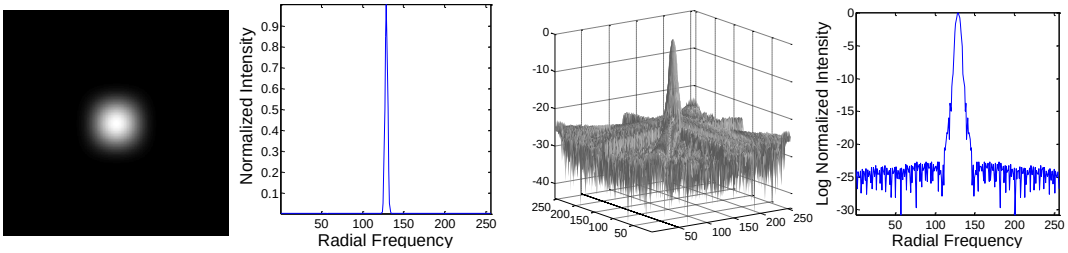

(a) (b) (c) (d)

Fig. 7: (a) Square apodize aperture at υ =5, (b) Central line through a normalized psf, (c) Logarithmic scale of a normalized psf, and (d) Central line through (c).

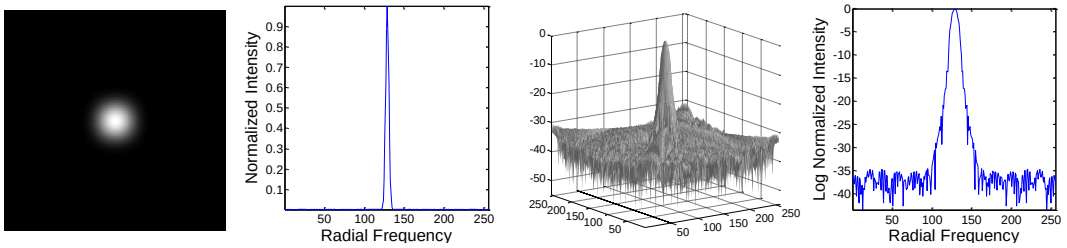

(a) (b) (c) (d)

Fig. 8: (a) Circular apodize aperture at υ =8, (b) Central line through a normalized psf, (c) Logarithmic scale of a normalized psf, and (d) Central line through (c).

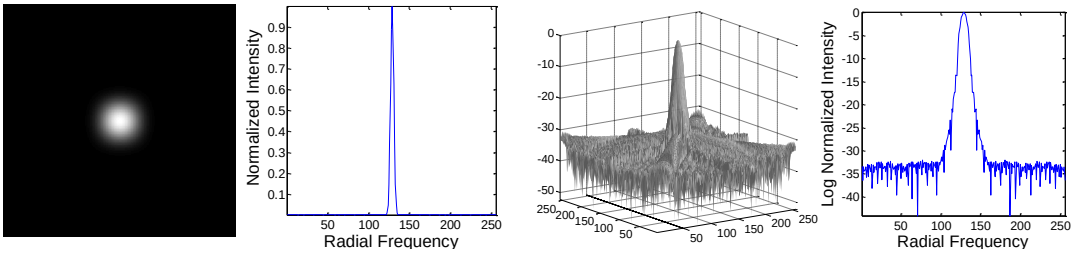

(a) (b) (c) (d)

Fig. 9: (a) Square apodize aperture at υ =8, (b) Central line through a normalized psf, (c) Logarithmic scale of a normalized psf, and (d) Central line through (c).

It is of interest now to compare the results that is obtained from implementing apodize circular and square apertures with that obtained with classical apertures. The central lines through a normalized logarithmic scale of the psf are shown in figure (10). It is very clear that with υ=8, the radial frequency components using apodize circular and square apertures decline very rapidly making the possibility of detecting extrasolar planets becomes high.

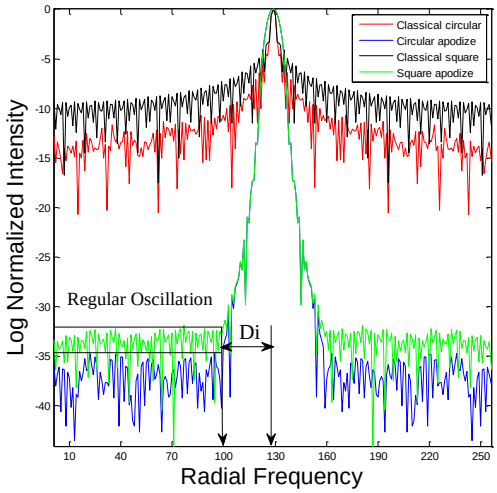

Fig. 10: Central line through logarithmic scale of a normalized psf using different apertures.

The quality of the apodize apertures depends on two properties. The first is the mean value (M) of the regular oscillation points that lie below the radial frequency of 100. The second is the distance (Di) from the center to the first oscillation point that the oscillation becomes regular, i.e. the distance from the center to radial frequency value of 100 (see figure 10). This value is visually chosen because it represents the separation value for the beginning of regular oscillations and considered to be a perfect value for calculating the full width of psf. The result of computing these properties is demonstrated in figure (11).

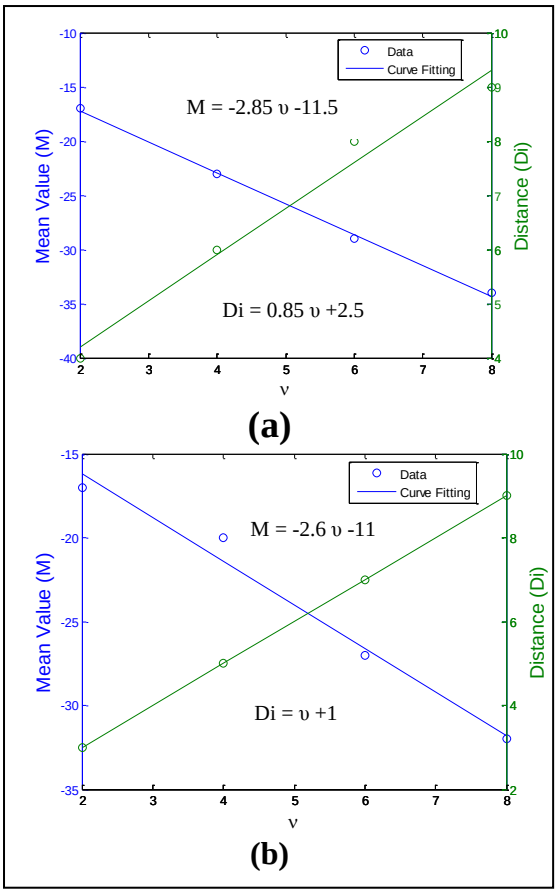

Fig. 11: (a) & (b) The relationship between mean value and distance of the logarithmic scale of the normalized psf for circular and square apodize apertures as a function of υ.

M & Di are one degree polynomial equations that fitted the data. It is clear from these figures that the mean value of the circular and square apodize apertures is inversely proportional with υ while the distance is linearly proportional with υ.

To assess the quality of these techniques in observing extrasolar planet by optical telescope, a binary system is generated as follows:

$$B(x,y) = A*e^{-((x-x_c)^2+(y-y_c+d)^2/(2*\sigma_1^2))} + e^{-((x-x_c)^2+(y-y_c-d)^2/(2*\sigma_2^2))} \quad \ldots(10)$$

where A is the brightness of the star while the reflected brightness of the planet kept constant at a value of one,

so that, the contrast ratio (CR) is the ratio of the brightness of the planet to the brightness of the star. This is equivalent to (1/A) and d is the separation distance between star & planet. d is taken to be 10 pixels to ensure the planet that lies beneath the wings of the radial frequency components of the psf of the optical telescope in use. σ_1 and σ_2 are the standard deviations of the star and the planet respectively and taken to be 2 pixels. The image of a binary system that could be observed by optical telescope is the convolution between equations (5) and (10) and represented by:

$$C(x,y)=\iint_{-\infty}^{\infty} B(x',y')psf(x-x',y-y')dx'dy' \quad \ldots(11)$$

This equation may also be written as:

$$C(x,y) = B(x, y) \otimes psf(x,y) \ldots(12)$$

where $\otimes$ denotes convolution operator. This equation demonstrates the observation of a star and planet by optical telescope in the absence of atmospheric turbulence and any geometrical aberration that contributed from the optical telescope. Logarithmic scale is then applied on the normalized results of a binary system. The results are demonstrated in figures (12 & 13).

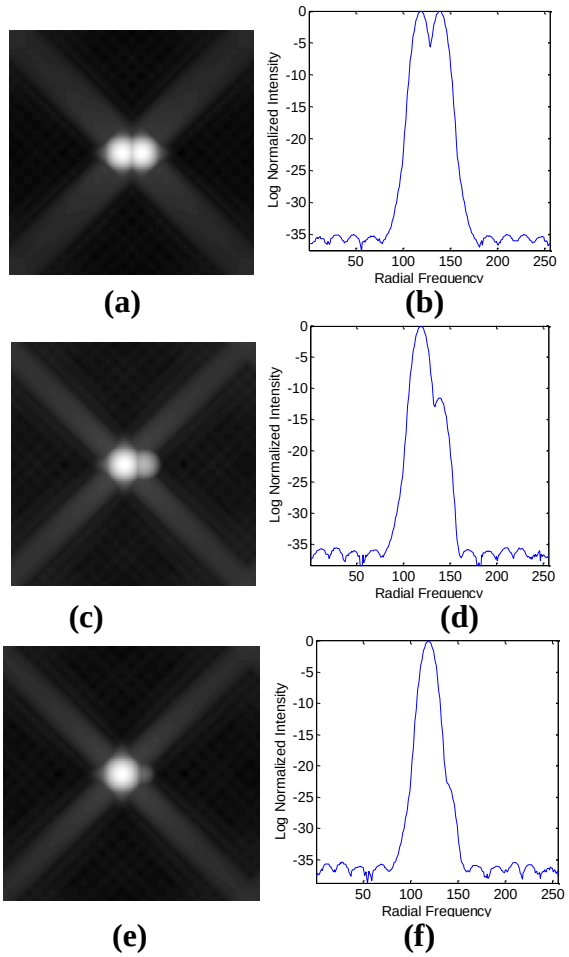

Fig. 12: Logarthmic image of a binary system with a circular apodize aperture at υ = 8 using different CR, a-CR=1, b- Centeral line through (a), c-CR=10^{-5}, d-Centeral line through (c), e - CR=10^{-10}, and f- Centeral line through (e).

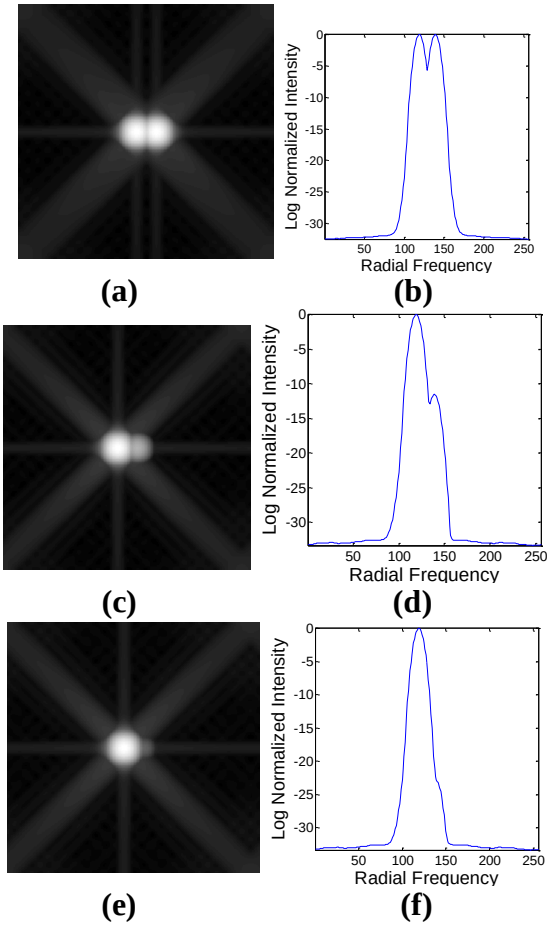

Fig. 13: Logarthmic image of a binary system with a square apodize aperture at υ = 8 using different CR, a-CR=1, b- Centeral line through (a), c-CR=10^{-5}, d-Centeral line through (c), e - CR=10^{-10}, and f- Centeral line through (e).

Now, we would like to study the effect of changing the separation of the binary system on the possibility of observing extrasolar planet. d are taken to be 30 and 5 pixels. This is to ensure that the planet is located near the edge and the center of the radial frequency. The results are shown in figures (14 and 15) respectively.

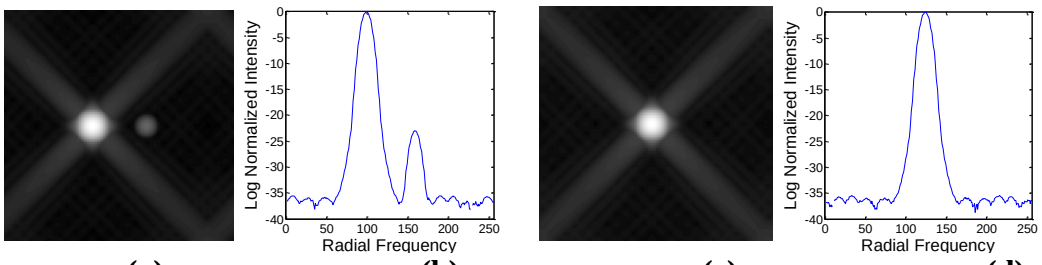

Fig. 14: Logarthmic image of a binary system using a circular apodize aperture at υ = 8 and CR=10^{-10}, a-Seperation =30 pixels, b- Centeral line through (a), c-Seperation =5 pixels, and d- Centeral line through (c).

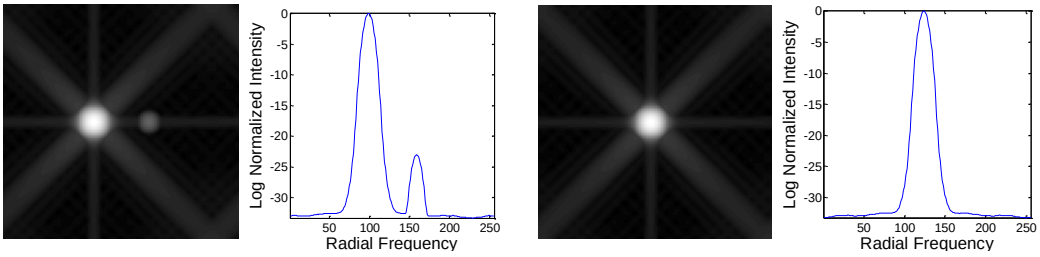

(a) (b) (c) (d)

Fig. 15: Logarthmic image of a binary system using a square apodize aperture at υ = 8 and CR=10^{-10}, a-Seperation =30 pixels, b- Centeral line through (a), c-Seperation =5 pixels, and d- Centeral line through (c).

Conclusions:

The important conclusions could be summarized as follows:

1. The circular apodize aperture with υ=8 makes the mean value of the wings of the logarithmic scale of the normalized psf around -34, while this mean becomes around -32 for square apodize aperture using the same value.
2. The circular apodize aperture reveals clearly the extrasolar planet even with CR = 10^{-10}, while with the square apodize aperture is hardly to be noticed.
3. The results also indicate that imaging extrasolar planet strongly depends on the separation between star and planet and the type of telescope aperture. It should be pointed out here that a tradeoff between the separation and the type of aperture must be made for enhancing the quality of imaging extrasolar planet.

References:

1. Swartzlander, G. A; Ford, E. L; Abdul-Malik, R. S; Close, L. M; Peters, M. A; Palacios, D. M and Wilson, D.W. 2008. Astronomical Demonstration of an Optical Vortex Coronograph, Optics Express. J. 16(14):10200-10207.

2. Carlotti, A; Vanderbei, R. and Kasdin, N.J. 2011. Optimal Pupil Apodization for Arbitrary Apertures for High Contrast Imaging, Optics Express. J. 19(27):26796-26809.

3. Lloyd, J. P; Graham, J. R; Kalas, P; Oppenheimer, B. R; Sivaramakrishnan, A. N; Makidon, R; Macintosh, B. A; Baudoz,C. M; Khun, J. and Potter, D. 2003. Astronomical Coronagraphy with High Order Adaptive Optics, Proceeding of Soci. Photo. Instru. Engine. (SPIE) Conference. 4860(1):315-322.

4. Ferrari, A; Soummer, R. and Aime, C. 2008. Introduction to Stellar Coronagraphy, Europ. Astron. Soci. J. 8(2):79-92.

5. Thompson, S. J; Doel, A. P; Bingham, R. G; Charalambous, A; Myers, R; Bissonauth, N; Clark, P. and Talbot, G. 2005. Results from the Adaptive Optics Coronagraph at the WHT, Mon. Not. R. Astro. Soci. J. 364(4):1203-1210.

6. Colón, K. D; Ford, E. B; Lee, B; Mahadevan, S. and Blake, C. H. 2010. Characterizing Transiting Extrasolar Planets with Narrow-Band Photometry and GTC/ OSIRIS, Mon. Not. R. Astro. Soci. J. 408(3):1449-1501.

7. Guyon, O; Pluzhnik, E; Martinache, F; Totems, J; Tanaka, S; Matsuo, T; Blain, C. and Belikov, R. 2010. High Contrast Imaging and Wavefront Control with a PIAA Coronograph: Laboratory System Validation, Proceeding of Astron. Soci. Pacific Conference. 122 (887) :71-84.

8. Lozi, J; Martinache, F. And Guyon, O. 2009. Phase-Induced Amplitude Apodization on Centrally Obscured Pupils: Design and First Laboratory Demonstration for the Subaru Telescope Pupil, Proceeding of Astron. Soci. Pacific Conference. 121(24):1232-1244.

9. Abe, L; Beaulieu,M; Vakili, F; Gay, J; Rivet, J. P; Dervaux, S. and Souza, A. D. 2007. On-Sky Observations with an Achromatic Hybrid Phase Knife Coronograph in the Visible, Astron. & Astroph. J. 461(3):365-371.

10. Basinger, S. and Redding, D. C. 2004. Terrestrial Planet Finder Coronagraph Optical Modeling, Proceeding of Astron. Soci. Pacific Conference. 5528(1):277-286.

11. Kenworthy, M. A; Quanz, S. P; Meyer, M. R; Kasper, M. E; Lenzen, R; Codona, J. L; Grard, J. H; and Hinz, P. M. 2010. An Apodizing Phase Plate Coronograph for VLT/NACO, Proceeding of Soci. Photo. Instru. Engine. (SPIE) Conference. 7735(3):77532-77541.

12. Heap, S. R; Lindler, D. J; Lanz, T. M; Cornett, R. H; Hubeny, I; Maran, S. P; and Woodgate, B. 2000. Space Telescope Imaging Spectrograph Coronagraphic Observations of β Pictoris, Astroph. J. 539(1):435- 444.

13. Enya, K; Kotani, T; Haze, K; Aono, A; Nakagawa, T; Matsuhara, H; Kataza, H; Wada, T; Kawada, M; Fujiwara, K; Mita, M; Takeuchi, S; Komatsu, K; Sakai, S; Uchida, H; Mitani, S; Yamawaki, T; Miyata, T; Sako, S; Nakamura, T; Asano, K; Yamashita, T; Narita, N; Matsuo, T; Tamura, M; Nishikawa, J; Kokubo, E; Hayano, Y; Oya, S; Fukagawa, M; Shibai, H; Baba, N; Murakami, N; Itoh, Y; Honda, M; Okamoto, B; Ida, S; Takami, M; Abe, L; Guyon, O; Bierden, P. and Yamamuro, T. 2011. The SPICA Coronagraphic Instrument (SCI) for the Study of Exoplanets, Advan. Spac. Resear. J. 48(2):323-333.

14. Hashimoto, J; Tamura, M; Muto, T; Kudo, T; Fukagawa, M; Fukue, T; Goto, M; Grady, C; Henning, T; Hodapp, K; Honda, M; Inutsuka, S; Kokubo, E; Knapp, G; Meclwain, M; Momose, M; Ohashi, N; Okamoto, Y; Takami, M; Turner, E; Wisniewski, J; Janson, M; Abe,L; Brander, W; Carson, J; Egner, S; Feldt, M; Golota, T; Guyon, O; Hayano, Y; Hayashi, M; Hayashi, S; Ishii, M; Kandori, R; Kusakabe, N; Matsuo, T; Mayama, S; Miyama, S; Morino, J; Martin, A; Nishimura, T; Pyo, T; Suto, H; Takato, N; Terada, H; Thalmann, C; Tomono, D; Watanabe, M; Yamada, T; Takami, H. and Usuda, T. 2011. Direct Imaging of Fine Structures in Giant Planet Forming Regions of the Protoplanetary Disk around AB Aurigae, Astroph. J. 729(2):L17-L29.

15. Rodrigues, G. M. 2010. Adaptive Optics with Segmented Deformable Bimorph Mirrors, Ph.D. Thesis, Department of Mechanical Engineering and Robotics. University of Libre De Bruxelles. PP.20-21.

16. Britton, T. R. 2009. High Dynamic Range Direct Imaging of Exoplanets with an Off-Axis Antarctic Telescope. M.Sc.Thesis. School of Physics. University of New South Wales. PP.26-27.

17. Aime, C; Soummer, R. and Ferrari, A. 2002. Total Coronagraphic Extinction of Rectangular Apertures using Linear Prolate Apodizations, Astron. & Astroph. J. 389(1):334-344.

18. Nisenson, P. and Papaliolios, C. 2001. Detection of Earth-Like Planets using Apodized Telescopes, Astroph. J. 548(2):L201-L205.

محاكاة عددية لتصوير الكواكب الخارجية باستخدام الفتحات الدائرية والمربعة الابودايزية

*علي طالب محمد** *عدي عطيوي جلود**

*قسم الفلك، كلية العلوم، جامعة بغداد، بغداد – الجادرية

الخلاصة:

تمت محاكاة عددية للفتحات الدائرية والمربعة الابودايزية وتقييم نوعيتها من خلال امكانية رصدها كواكب قريبة من النجوم. اظهرت النتائج ان مركبات التردد النصف قطرية تهبط الى 10^{-36} بالنسبة للفتحات الدائرية و10^{-34} بالنسبة للفتحات المربعة الابودايزية وهذا يصاحبة ايضاً زيادة في عرض دالة النتشار النقطية. يجب اجراء بعض التوافق بين قيم الهبوط في الترددات النصف قطرية وعرض دالة النتشار النقطية للتغلب على مشكلة تصوير الكواكب الخارجية.